Modeling the morphogenesis of brine channels in sea ice

B. Kutschan
Ident Technologies GmbH, Rudower Chaussee 29, 12489 Berlin, Germany

K. Morawetz
Münster University of Applied Science, Stegerwaldstrasse 39, 48565 Steinfurt, Germany
and International Center for Condensed Matter Physics, Universidade de Brasília, 70904-910 Brasília, DF, Brazil

S. Gemming
Forschungszentrum Dresden-Rossendorf, PF 51 01 19, 01314 Dresden, Germany

(Received 28 July 2009; revised manuscript received 23 December 2009; published 15 March 2010)

Brine channels are formed in sea ice under certain constraints and represent a habitat of different microorganisms. The complex system depends on a number of various quantities as salinity, density, pH value, or temperature. Each quantity governs the process of brine channel formation. There exists a strong link between bulk salinity and the presence of brine drainage channels in growing ice with respect to both the horizontal and vertical planes. We develop a suitable phenomenological model for the formation of brine channels both referring to the Ginzburg-Landau theory of phase transitions as well as to the chemical basis of morphogenesis according to Turing. It is possible to conclude from the critical wave number on the size of the structure and the critical parameters. The theoretically deduced transition rates have the same magnitude as the experimental values. The model creates channels of similar size as observed experimentally. An extension of the model toward channels with different sizes is possible. The microstructure of ice determines the albedo feedback and plays therefore an important role for large-scale global circulation models.

DOI: 10.1103/PhysRevE.81.036106 PACS number(s): 82.40.Ck, 92.05.Hj, 89.75.Kd, 47.54.−r

I. INTRODUCTION

Formation and decay of complex structures depend on changes in entropy. In the long run, structures tend to decay since the entropy of universe leads to a maximum and evolves into a "dead" steady state [1]. On the other hand, not only living cells avoid the global thermodynamic equilibrium. Turing [2] showed in his paper about the chemical basis of morphogenesis which additional conditions are necessary to develop a pattern or structure. For instance, cells can be formed due to an instability of the homogeneous equilibrium which is triggered by random disturbances. In this sense, it should be possible that the habitat of microorganisms in polar areas, the brine channels in sea ice, can be described through a Turing structure.

The internal surface structure of ice changes dramatically when the ice cools below −23 °C or warms above −5 °C and has a crucial influence on the species composition and distribution within sea ice [3,4]. This observation correlates with the change of the coverage of organisms in brine channels between −2 and −6 °C [4]. Golden *et al.* [5] found a critical brine volume fraction of 5% or a temperature of −5 °C for salinity of 5 parts per thousand where the ice distinguishes between permeable and impermeable behaviors concerning energy and nutrient transports. According to Perovich and Gow [6], the brine volume increases from 2 to 37‰ and the correlation length increases from 0.14 to 0.22 mm if the temperature rises from −20 to −1 °C. The permeability varies over more than 6 orders of magnitude [7]. Whereas Golden *et al.* [5] used a percolation model, we will demonstrate how the brine channel distribution can be modeled by a reaction-diffusion equation similar to the Ginzburg-Landau treatment of phase transitions. A molecular-dynamics simulation shows the change between the hexagonal-arranged ice structure and the more disordered liquid water structure [8].

After a short introduction into the key issue of the structure formation, we describe the brine channel structure in sea ice and propose a phenomenological description. For the interpretation of the order parameter, we discuss some microscopic properties of water using molecular-dynamics simulation in Sec. II. In Sec. III, we consider the phase transition and the conditions which allow a structure formation. We verify the model on the basis of measured values in Sec. IV and give finally an outlook on further investigations in Sec. V.

II. MICROSCOPIC PROPERTIES OF WATER

A. Formation of brine channels

Various publications report on the life condition for different groups of organisms in the polar areas in brine-filled holes, which arise under certain boundary conditions in sea ice as base or brine channels (lacuna) [9–11]. They are characterized by the simultaneous existence of different phases, water, and ice in a saline environment. Because already marginal temperature variations can disturb this sensitive system, direct measurements of the salinity, temperature, pH value, or ice crystal are morphologically difficult [9]. Weissenberger *et al.* [12] developed a cast technique in order to examine the channel structure. Freeze drying eliminates the ice by sublimation and the hardened casts illustrate the channels as negative pattern. Figure 1 shows a typical granular texture without prevalent orientation.

Sometimes, both columnar and mixed textures occur. Using an imaging system, Light *et al.* [3] found brine tubes, brine pockets, bubbles, drained inclusions, transparent areas,

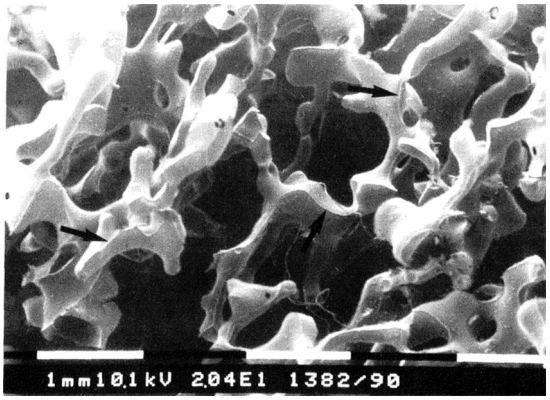

FIG. 1. Scanning electron microscopy (SEM) image of a cast of brine channels [9].

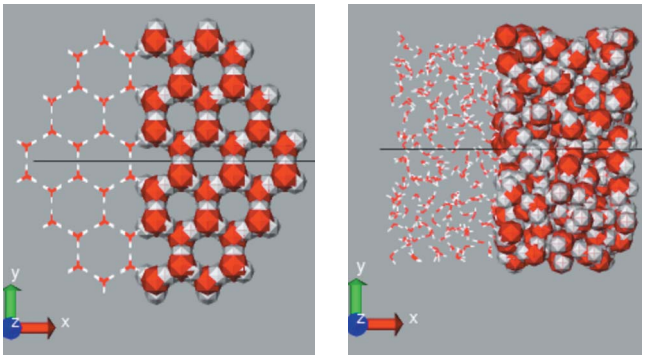

FIG. 2. (Color online) Hexagonal ice (left) and liquid water at 300 K (right).

and poorly defined inclusions. Air bubbles are much larger than brine pockets. Bubbles possess a mean major axis length of some millimeters and brine pockets are hundred times smaller [13]. Cox *et al.* [14–16] presented a quantitative model approach investigating the brine channel volume, salinity profile, or heat expansion but without pattern formation. They also described the texture and genetic classification of the sea ice structure experimentally. A crucial factor for the brine channel structure formation is the spatial variability of salinity [17].

Different mechanisms are employing the mobility of brine channels which can be used to measure the salinity profile [17]. Advanced microscale photography has been developed to observe *in situ* the distribution of bottom ice algae [18] which allows determining the variability of the brine channel diameter from bottom to top of the ice. By mesocosm studies, the hypothesis was established that the vertical brine stability is the crucial factor for ice algae growth [19]. Therefore, the channel formation during solidification and its dependence on the salinity is of great interest both experimentally and theoretically [20]. Experimentally, Cottier *et al.* [17] presented images, which show the linkages between salinity and brine channel distribution in an ice sample.

To describe different phases in sea ice dependent on temperature and salinity, one possible approach is based on the reaction-diffusion system

$$\frac{\partial \boldsymbol{w}(\boldsymbol{x},t)}{\partial t} = \boldsymbol{f}(\boldsymbol{x},t) + \boldsymbol{D}\boldsymbol{\nabla}^2 \boldsymbol{w}(\boldsymbol{x},t), \tag{1}$$

where $\boldsymbol{w}=\binom{u}{v}$ is the vector of reactants, $\boldsymbol{x}=(x,y,z)$ is the three-dimensional space vector, $\boldsymbol{f}$ is the nonlinear reaction kinetics, and $\boldsymbol{D}=\left(\begin{smallmatrix} D_1 & 0 \\ 0 & D_2 \end{smallmatrix}\right)$ is the matrix of diffusitivities, where $\boldsymbol{D_1}$ is the diffusion coefficient of water and $\boldsymbol{D_2}$ is the diffusion coefficient of salt. For the one- and two-dimensional cases, we set $\boldsymbol{y}=\boldsymbol{z}=\boldsymbol{0}$, respectively, $\boldsymbol{z}=\boldsymbol{0}$. The reaction kinetics described by $\boldsymbol{f}(\boldsymbol{x},t)$ can include the theory of phase transitions by Ginzburg-Landau for the order parameters. Referring to this, Fabrizio [21] presented an ice-water phase transition. Under certain conditions, spatial patterns evolve in the so-called Turing space. These patterns can reproduce the distribution ranging from sea water with high salinity to sea ice with low salinity. The brine channel system exists below a critical temperature in a thermodynamical nonequilibrium. It is driven via the desalination of ice during the freezing process that leads to a salinity increase in the brine channels. The higher salt concentration in the remaining liquid phase leads to a freezing point depression and triggers the ocean currents.

B. Different states of water

Already Röntgen had described the anomalous properties of water with molecules of the first kind, which he called ice molecules and molecules of the second kind [22] and which represent the liquid aggregate state. Dennison [23] determined the ordinary hexagonal ice-I modification from x-ray pattern methodically verified by Bragg [24]. This so-called E_h ice is formed by four oxygen atoms which build a tetrahedron as illustrated in Fig. 2. In E_h ice, each oxygen atom is tetrahedrically coordinated by four neighboring oxygen atoms, each accompanied by a hydrogen bridge. The arrangement is isomorphous to the wurtzite form of zinc sulphide or to the silicon atoms in the tridymite form of silicon dioxide. Bjerrum [25] and Eisenberg and Kauzmann [26] provided a survey about the structure differences between the different polymorphic forms of ice and liquid water.

Molecular dynamics simulations with the three-site transferable intermolecular potential model of water using the nanoscale molecular dynamics software by the Theoretical and Computational Biophysics Group of the University of Illinois show the change from a regular hexagonal lattice structure to irregular bonds after the melting (Fig. 2). Nada *et al.* [8] developed a better six-site potential model of H_2O for a crystal growth of ice from water using molecular dynamics and Monte Carlo methods. They computed both the free energy and an order parameter for the description of the water structure. Also Medvedev and Naberukhin [27] introduced a "tetrahedricity measure" M_T for the ordering degree of water. It is possible to discriminate between ice and water molecules via a two-state function ($G=0$ if $M_T \geq M_T^c$ and $G=1$ if $M_T < M_T^c$). This tetrahedricity is computed using the sum

$$M_T = \frac{1}{15\langle l^2 \rangle} \sum_{i,j} (l_i - l_j)^2, \tag{2}$$

where l_i are the lengths of the six edges of the tetrahedron formed by the four nearest neighbors of the considered water

molecule. For an ideal tetrahedron, one has $M_T=0$ and the random structure yields $M_T=1$. The tetrahedricity can be used in order to define an order parameter according to the Landau–de Gennes model for liquid crystals, which refers to the Clausius-Mosotti relation. Other simulations such as the percolation models of Stanley *et al.* [28,29] use a two-state model, in which a critical correlation length determines the phase transition. A mesoscopic model for the sea ice crystal growth is developed by Kawano and Ohashi [30] who used a Voronoi dynamics.

III. REACTION-DIFFUSION MODEL

A. 1+1-dimensional model equations

We consider the reaction-diffusion system

$$\frac{\partial u(x,t)}{\partial t} = a_1 u - c u^3 + d u^5 + b_1 v + D_1 \frac{\partial^2 u(x,t)}{\partial x^2}, \tag{3}$$

$$\frac{\partial v(x,t)}{\partial t} = -a_2 v - b_2 u + D_2 \frac{\partial^2 v(x,t)}{\partial x^2} \tag{4}$$

in one space dimension. The order parameter according to the Ginzburg-Landau theory is $u(x,t)$ with $u_{min} \le u_c \le u_{max}$ and proportional to the tetrahedricity $u \sim M_T$. If the variable u is smaller than u_c ($u < u_c$), the phase changes from water to ice and vice versa. Thus, changes in u reflect temperature variations. The variable v is a measure of the salinity. The coefficient a_1 depends on the temperature T as $(T-T_c)/T_c$ with the critical temperature T_c. The salt exchange between ice and water is realized by the gain term $b_1 v$ and the loss term $-a_2 v$. The positive terms $a_1 u$ and $b_1 v$ are the temperature- and salt-concentration-dependent "driving forces" of the system.

In order to realize the T-dependent phase transition, one can expand the order parameter in a power series corresponding to Ginzburg and Landau in Eq. (3). In order to describe properly a temperature-induced phase transition of second order, an expression $-cu^3$ is necessary. The first-order phase transition is dependent on du^5. Supercooled or superheated phases can coexist, i.e., a hysteresis behavior is possible. Without the term du^5, we can also realize a brine channel formation. But this second-order phase transition does not allow us to consider the specific heat as a jump in the order parameter ψ (Figs. 3 and 4). We write Eqs. (3) and (4) in dimensionless form (see Appendix A) by setting $\tau = \sqrt{b_1 b_2}\, t$, $\xi = \sqrt[4]{b_1 b_2 / D_1^2}\, x$, $\psi = \sqrt[4]{c^2 / b_1 b_2}\, u$, and $\rho = \sqrt[4]{b_1 c^2 / b_2^3}\, v$ and get

$$\frac{\partial \psi(\xi,\tau)}{\partial \tau} = f[\psi,\rho] + \frac{\partial^2 \psi(\xi,\tau)}{\partial \xi^2}, \tag{5}$$

$$\frac{\partial \rho(\xi,\tau)}{\partial \tau} = g[\psi,\rho] + D \frac{\partial^2 \rho(\xi,\tau)}{\partial \xi^2}, \tag{6}$$

with $\alpha_1 = a_1/\sqrt{b_1 b_2}$, $\delta = d\sqrt{b_1 b_2}/c^2$, $\alpha_2 = a_2/\sqrt{b_1 b_2}$, and $D = D_2/D_1$ as well as the reaction kinetics

$$f[\psi,\rho] = \alpha_1 \psi - \psi^3 + \delta \psi^5 + \rho, \tag{7}$$

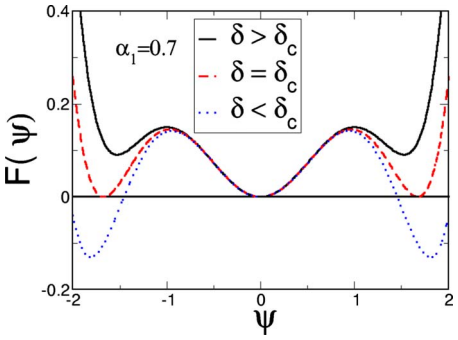

FIG. 3. (Color online) Landau function (9) vs the dimensionless order parameter (tetrahedricity) for various δ.

$$g[\psi,\rho] = -\alpha_2 \rho - \psi, \tag{8}$$

where ψ is the dimensionless order parameter of the water-ice system and ρ the dimensionless salinity. Thus, the dynamics only depends on four parameters α_1, α_2, δ, and D. Without the salinity ρ in Eq. (3), respectively, Eq. (5), the above equation system is reduced to a Ginzburg-Landau equation for the first-order phase transition.

First-order phase transitions

When we neglect the salinity ρ, the integration of the kinetic function (7) yields the Landau function for the order parameter ψ of water-ice

$$F = \frac{a_1}{2}\psi^2 - \frac{1}{4}\psi^4 + \frac{\delta}{6}\psi^6 \tag{9}$$

as plotted in Fig. 3. It possesses three minima

$$\psi_{\min} = \left\{ 0, \pm \sqrt{\frac{1}{2\delta}(1 + \sqrt{1 - 4\delta\alpha_1})} \right\}. \tag{10}$$

When several different minima of equal depth exist, then there is a discontinuity in ψ due to Maxwell construction and one has a first-order phase transition [31]. This is the case if

$$\delta = \delta_c = \frac{3}{16\alpha_{1c}} \tag{11}$$

and

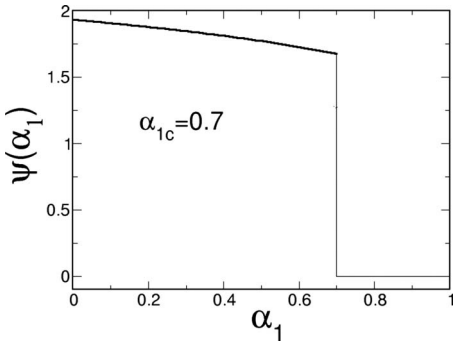

FIG. 4. The minimal order parameter $\psi_{\min}$ of Eq. (10) dependent on α_1.

$$\psi_c^2 = \frac{3}{4\delta_c}, \tag{12}$$

in consequence of

$$F = \psi^2\left[\frac{\delta}{6}\left(\psi^2 - \frac{3}{4\delta}\right)^2 + \frac{\alpha_1}{2} - \frac{3}{2\cdot 16\delta}\right] = 0. \tag{13}$$

Thus the critical parameter $\delta=\delta_c$ is determined by the temperature-dependent critical value $\alpha_1=\alpha_{1c}$. The jump in Figs. 3 and 4 is a measure for the latent heat of the phase transition from water to ice. Feistel and Hagen [32] deduced theoretically the latent heat of sea ice for various salinities.

B. Linear stability analysis

First, we perform a linear stability analysis by linearizing the equation systems (5) and (6) according to $\psi=\psi_0+\bar{\psi}$ and $\rho=\rho_0+\bar{\rho}$. We obtain the characteristic equation for the fixed points with

$$\begin{pmatrix}\bar{\psi}\\ \bar{\rho}\end{pmatrix} = \begin{pmatrix}\bar{\psi}_i\\ \bar{\rho}_i\end{pmatrix}\exp(\lambda(\kappa)\tau + i\kappa\xi) \tag{14}$$

as

$$\begin{pmatrix}\frac{\partial}{\partial\tau}\bar{\psi}\\ \frac{\partial}{\partial\tau}\bar{\rho}\end{pmatrix} = \begin{pmatrix}\alpha_1 - 3\psi_0^2 + 5\delta\psi_0^4 & 1\\ -1 & -\alpha_2\end{pmatrix}\begin{pmatrix}\bar{\psi}\\ \bar{\rho}\end{pmatrix} + \begin{pmatrix}\frac{\partial^2}{\partial\xi^2} & 0\\ 0 & D\frac{\partial^2}{\partial\xi^2}\end{pmatrix} \times \begin{pmatrix}\bar{\psi}\\ \bar{\rho}\end{pmatrix}, \tag{15}$$

as outlined in Appendix B.

There are five fixed points for the kinetics (7) and (8) which satisfy $f=0$ and $g=0$. In order to get a stable nonoscillating pattern, we need a stable spiral point as fixed point. Moreover, the associated eigenvalues have to possess a positive real part for a positive wave number, i.e., they have to allow to create unstable modes. Not each fixed point satisfies both conditions. Therefore, for the following discussion, we choose the steady state, $\psi_0=0$ and $\rho_0=0$, which corresponds to the observable brine channel structures measured by a casting experiment [17,18].

Short-time experiments may also record structures that are formed under nonsteady conditions. Since those structures are beyond the scope of the present paper, we proceed with the steady state which leads from Eq. (15) to

$$\lambda(\kappa)^2 + [\kappa^2(1+D) + \alpha_2 - \alpha_1]\lambda(\kappa) + h(\kappa^2) = 0, \tag{16}$$

with

$$h(\kappa^2) = D\kappa^4 + (\alpha_2 - \alpha_1 D)\kappa^2 - \alpha_1\alpha_2 + 1 \tag{17}$$

and which is readily solved

$$\lambda(\kappa)_{1,2} = \frac{1}{2}\{\alpha_1 - \alpha_2 - (1+D)\kappa^2 \pm \sqrt{[\alpha_1 + \alpha_2 + (D-1)\kappa^2]^2 - 4}\}. \tag{18}$$

C. Turing space

Let us discuss Eqs. (16) and (17) concerning the conditions for the occurrence of Turing structures in detail. First, we concentrate on the situation $\kappa=0$ where a homogeneous phase is formed. Then, the fixed points $\psi=0$ and $\rho=0$ are stable according to the eigenvalues (18) if

$$\lambda_{1,2}(0) = -\frac{\alpha_2 - \alpha_1}{2} \pm \frac{1}{2}\sqrt{(\alpha_1 - \alpha_2)^2 - 4(1 - \alpha_1\alpha_2)} \tag{19}$$

are negative, otherwise we would have a globally unstable situation which we rule out. Also, homogeneous oscillations do not describe a brine channel formation. It is easy to see that the solution (19) gives only two negative values if

$$\text{condition I:} \quad \alpha_2 > \alpha_1 \ \text{ and } \ \alpha_1\alpha_2 < 1. \tag{20}$$

The trajectories of salinity ρ and the order parameter ψ converge to the steady-state value zero by damped oscillations. Therefore, the structure formation does not follow from the initial condition in time but from the range of the interaction in space.

Next we discuss the spatial inhomogeneous case, $\kappa^2>0$, where some spatial fluctuations may be amplified and form macroscopic structures, i.e., the Turing structure. Therefore, we search for such modes of Eq. (18) which grow in time, i.e., $\mathrm{Re}\,\lambda(\kappa)>0$. Time oscillating structures appear if $\mathrm{Im}\,\lambda(\kappa)\neq 0$, which can be seen from the solution of Eq. (18) to be the case if $\alpha_1+\alpha_2-2<(1-D)\kappa^2<\alpha_1+\alpha_2+2$. In this region, we have

$$\mathrm{Re}\,\lambda_{\mathrm{osc}}(\kappa) = \frac{\alpha_1 - \alpha_2 - \kappa^2(1+D)}{2}. \tag{21}$$

Demanding to be positive means $\kappa^2(1+D)<\alpha_1-\alpha_2$. Due to Eq. (20), this cannot be fulfilled since the diffusion constant D is positive and κ real. Therefore for a time-growing mode, we do not have an imaginary part of λ in our model. In other words, we do not have oscillating and time-growing structures. The restriction for the only allowed region is

$$|(1-D)\kappa^2 - \alpha_1 - \alpha_2| > 2. \tag{22}$$

In this region, we search now for the condition $\lambda>0$. The term before the square in Eq. (18) is negative as can be seen from Eq. (20). Therefore, we can only have positive λ if the square of this term is less than the content of the root. This leads to

$$(\alpha_1 - \kappa^2)(\alpha_2 + D\kappa^2) > 1, \tag{23}$$

which restricts the κ region to the interval

$$\kappa^2 \in \frac{1}{2D}(\alpha_1 D - \alpha_2 \pm \sqrt{(\alpha_1 D + \alpha_2)^2 - 4D}). \tag{24}$$

Due to Eq. (20), the term under the square root is smaller than the square of the first term in Eq. (24) and we get only a meaningful condition from Eq. (24) if

$$\alpha_1 D > \alpha_2. \tag{25}$$

Moreover, the square root must be real, i.e.,

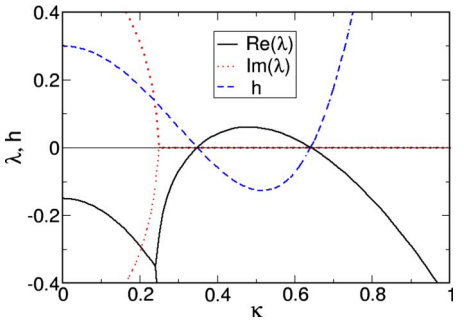

FIG. 5. (Color online) Dispersion of the linear stability (18) vs the dimensionless wave number κ for $\alpha_1=0.7$, $\alpha_2=1$, and $D=6$ together with the function $h(\kappa)$ of Eq. (17).

$$(\alpha_1 D+\alpha_2)^2-4D>0, \tag{26}$$

which leads to

$$D<\frac{(1-\sqrt{1-\alpha_1\alpha_2})^2}{\alpha_1^2} \quad \text{or} \quad D>\frac{(1+\sqrt{1-\alpha_1\alpha_2})^2}{\alpha_1^2}. \tag{27}$$

This has to be in agreement with Eq. (25) and discussing the different cases results finally into

$$\text{condition II:} \quad D>\frac{(1+\sqrt{1-\alpha_1\alpha_2})^2}{\alpha_1^2}. \tag{28}$$

Having determined the ranges of α_1, α_2, and D, we have to inspect the two conditions on κ, i.e., Eqs. (24) and (22). Discussing separately the cases $D \gtrless 1$, one sees that Eq. (22) gives no restriction on Eq. (24).

Collecting now all conditions for the occurrence of a Turing structure, Eqs. (28), (20), and (24), we obtain

$$\text{condition I:} \quad \alpha_2 \geq \alpha_1 \quad \text{and} \quad \alpha_1\alpha_2 \leq 1,$$

$$\text{condition II:} \quad D \geq \frac{(1+\sqrt{1-\alpha_1\alpha_2})^2}{\alpha_1^2},$$

$$\text{condition III:} \quad \kappa^2 \in \frac{1}{2D}[\alpha_1 D-\alpha_2 \pm \sqrt{(\alpha_1 D+\alpha_2)^2-4D}]. \tag{29}$$

The Turing space as phase diagram is determined by conditions I and II and is plotted in Fig. 6. One can see that the Turing space starts at the minimal (tricritical point)

$$\alpha_{1t}=\alpha_{2t}=D_t=1, \tag{30}$$

which means that we have only a Turing space for sufficient large diffusivity $D \geq 1$. For the Turing space, we obtain the possible wave numbers according to condition III as plotted in Fig. 7.

D. Critical modes

The critical wave number can be found from the largest modes. These are given by the minimum of Eq. (17) from which we find the wave numbers

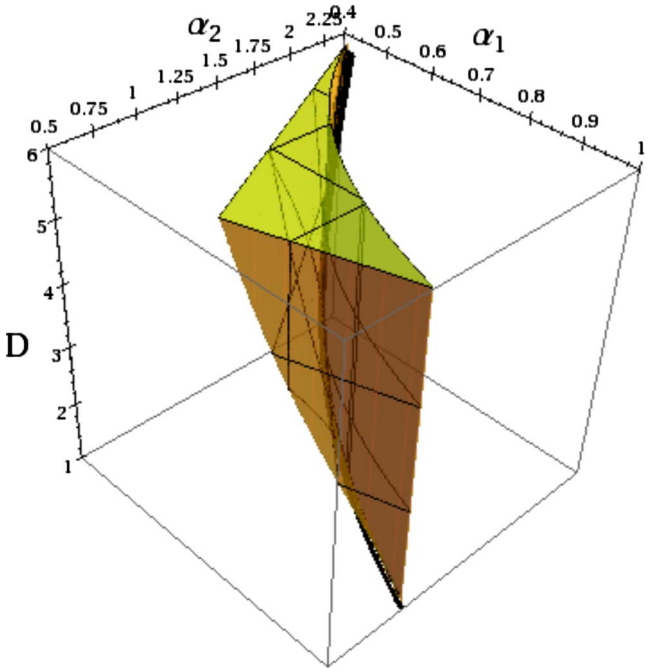

FIG. 6. (Color online) The Turing space as phase diagram where spatial structures can occur. The lower limiting line, $\alpha_2=1/\alpha_1$, $D=1/\alpha_1^2$, is plotted as thick line.

$$\kappa_{min}^2=\frac{1}{2D}(Df_\psi+g_\rho)=\frac{1}{2D}(D\alpha_1-\alpha_2) \tag{31}$$

and the minima

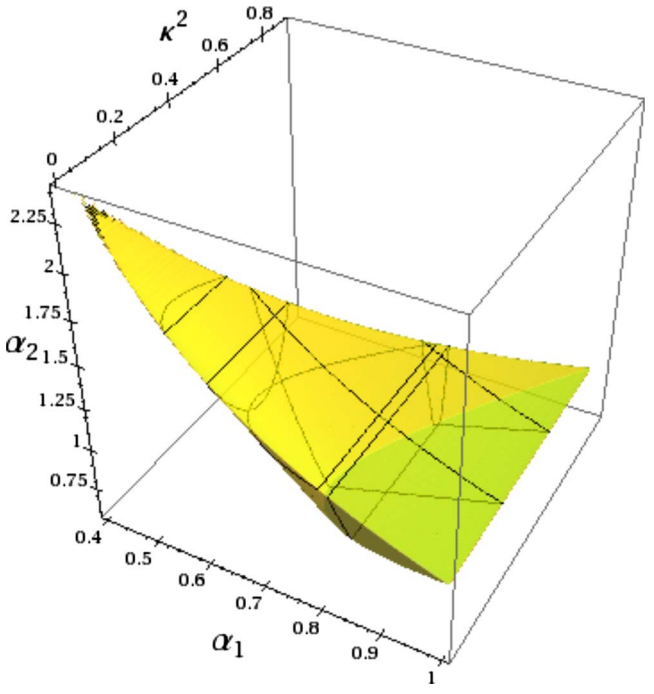

FIG. 7. (Color online) The possible wavelengths κ^2 where spatial structures can occur for $D=6$ in dependence on α_1 and α_2.

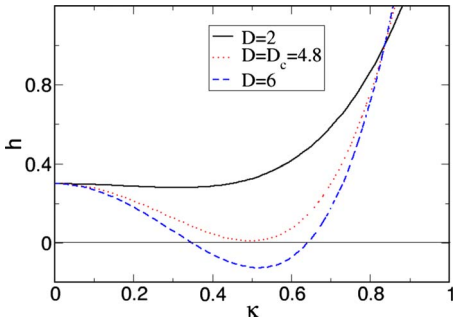

FIG. 8. (Color online) Dispersion $h(\kappa)$ for different D, $\alpha_1=0.7$, and $\alpha_2=1$.

$$h_{min} = f_\psi g_\rho - g_\psi f_\rho - \frac{(Df_\psi + g_\rho)^2}{4D} = 1 - \frac{(D\alpha_1 + \alpha_2)^2}{4D}. \quad (32)$$

For $\kappa^2_{min}>0$ and $h_{min}<0$, we find again the corresponding inequalities (25) and (26). The formation of a spatial Turing structure, a nonoscillating pattern, requires a negative h_{min} for $\kappa^2_{min}>0$. In this case, there is a range of wave numbers which are linearly unstable as seen in Fig. 5. In Fig. 8, we illustrate the behavior of $h(\kappa)$ for different diffusion constants. Only those which lead to negative h are forming the Turing structure as discussed in the previous chapter. This critical range can be obtained if the diffusion coefficient D is greater than the critical diffusion coefficient of condition II, Eq. (29) D_c,

$$D_c = \frac{(1+\sqrt{1-\alpha_1\alpha_2})^2}{\alpha_1^2}, \quad (33)$$

which we get from $h_{min}=0$ with the critical wave number κ_c,

$$\kappa_c^2 = \frac{D_c f_\psi + g_\rho}{2D_c} = \frac{D_c\alpha_1 - \alpha_2}{2D_c}. \quad (34)$$

The size of the structure can be estimated from $\frac{2\pi}{\kappa_c}$. The pattern size depends on the both parameters α_1 and α_2. The parameters determine the brine channel size and vice versa. With the parameters chosen in Fig. 5, we obtain a pattern size of 12.6. In the next chapter, we compare this value to experimental quantities. With a small initial random perturbation, we plot snapshots of the time evolution of the order parameter ψ and the salinity ρ in Fig. 9. The quantities ψ and ρ are opposite to each other; domains with low salinity correspond to domains with ice and domains with high salinity to water domains. We see the formation of a mean mode given by the wavelength κ_c.

A positive $h(\kappa=0)$, respectively, a negative $\lambda(\kappa=0)$, for $\kappa=0$ guarantees that ρ and ψ converge to the stable fixed point $\rho_0=0$, $\psi_0=0$. Therefore, the structure formation does not follow from the initial oscillations in time (Fig. 10). In order to obtain a new spatial structure, there must exist at least a negative h for $\kappa>0$, respectively, a positive eigenvalue λ, for $\kappa>0$ as was discussed in the last section.

E. 2+1-dimensional model

From the characteristic equation in the spatially two-dimensional case

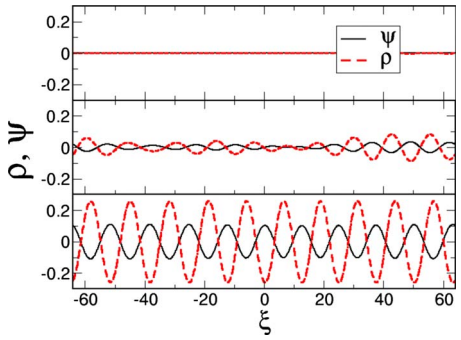

FIG. 9. (Color online) Time evolution of the order parameter ψ and salinity ρ vs spatial coordinates for $\tau=100$, 170, and 400 (from above to below) for $\alpha_1=0.7$, $\alpha_2=1$, $\delta=\frac{3}{16\alpha_1}$, and $D=6$ with the initial condition $\rho(\tau=0)=0.5\pm0.01N(0,1)$ and periodic boundary conditions.

$$\lambda^2 + [(\kappa_\xi^2+\kappa_\eta^2)(1+D)+\alpha_2-\alpha_1]\lambda + h(\kappa_\xi^2,k_\eta^2) = 0, \quad (35)$$

we find the corresponding dispersion relation

$$h(\kappa_\xi^2,\kappa_\eta^2) = D(\kappa_\xi^2+\kappa_\eta^2)^2 + (\alpha_2-\alpha_1 D)(\kappa_\xi^2+\kappa_\eta^2) - \alpha_1\alpha_2 + 1 \quad (36)$$

which is illustrated in Fig. 11.

The Turing space is bounded by the sectional plane $h=0$. The evolution of the order parameter ψ and the salinity ρ is illustrated in Figs. 12 and 13. Their behavior is inversely proportional and corresponds to the fact that a high salinity occurs in the water phase and a low salinity in the ice phase. Similar as in the one-dimensional case, we see the dominant formation of one wavelength. The model kinetics generate brine channels of similar size. In order to obtain a hierarchical net of brine channels of different size, the kinetics in the basic equations can be altered accordingly [33].

F. Note on second- and third-order kinetics

If we replace the kinetics (7) by

$$f[\psi,\rho] = \alpha_1\psi - \psi^3 + \rho \quad (37)$$

or

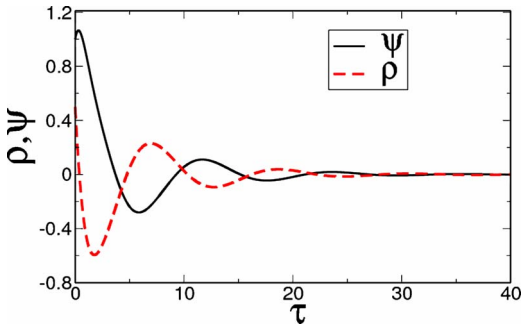

FIG. 10. (Color online) Time evolution of the order parameter ψ and the salinity ρ for $\alpha_1=0.7$, $\alpha_2=1$, $\delta=\frac{3}{16\alpha_1}$, and the initial order parameter $\psi(\tau=0)=1$ and the dimensionless salinity $\rho(\tau=0)=0.5$.

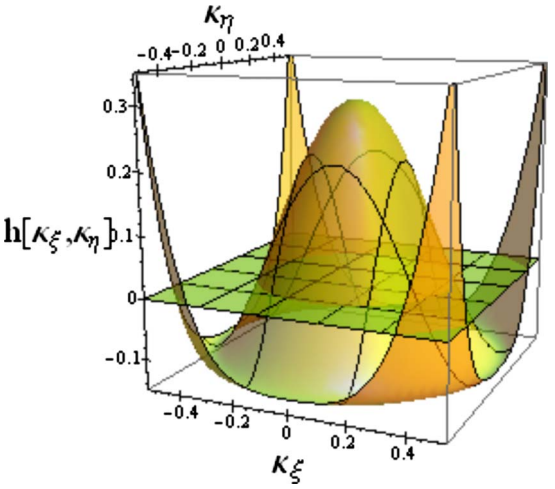

FIG. 11. (Color online) Dispersion of the two-dimensional characteristics (35) and (36) for $\alpha_1=0.7$, $\alpha_2=1$, and $D=6$.

$$f[\psi,\rho]=\alpha_1\psi-\psi^2+\rho, \tag{38}$$

we can carry out the same linear stability analysis for the fixed point $\psi_0=0$ and $\rho_0=0$. Then we obtain the same characteristic equation as Eqs. (16) and (17). Therefore, we get the same Turing space for the structure formation. Consequently, both kinetics allow us to realize a brine channel formation but the third-order kinetics describes a second-order phase transition only. In this connection, it is possible to discuss second-order phase transitions with spin models too.

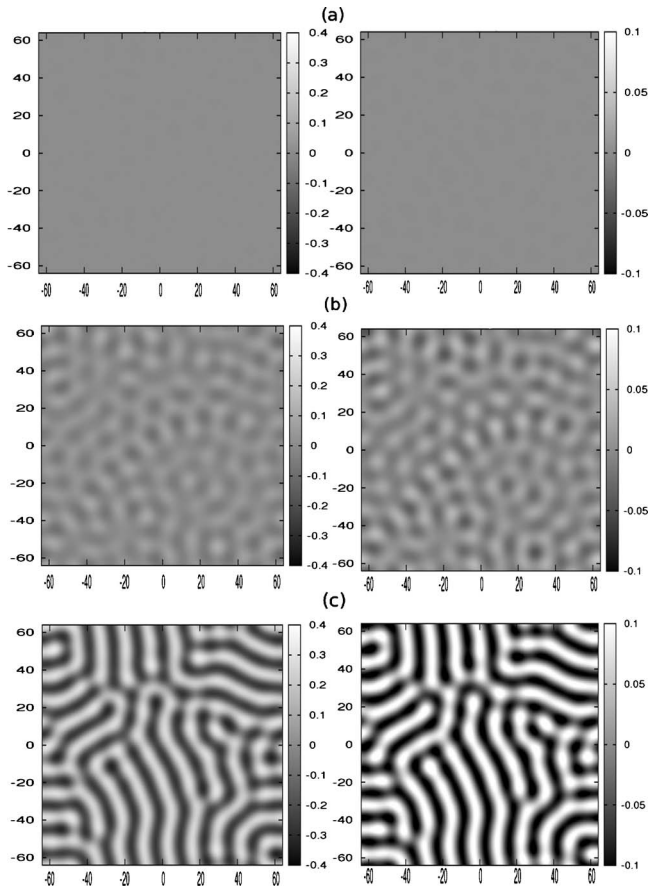

FIG. 12. Structure formation for three time steps $\tau=100$, 170, and 400 [from top to bottom (a)–(c)] for the order parameter Ψ (left) and the salinity ρ (right). The parameters are $\alpha_1=0.7$, $\alpha_2=1$, $\delta=\frac{3}{16a_1}$, and $D=6$ with the initial condition $\rho(\tau=0)=0.5\pm0.01N(0,1)$ and periodic boundary conditions.

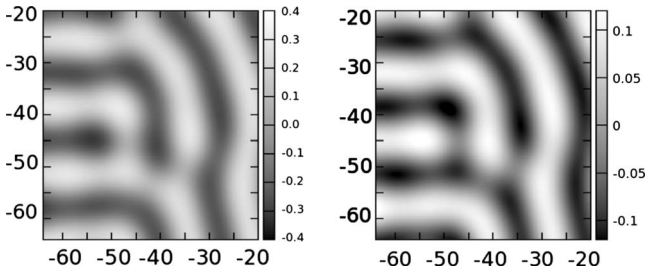

FIG. 13. Magnification of a detail of Fig. 12 for $\tau=400$.

IV. CONNECTION TO EXPERIMENTAL DATA

The critical domain size is determined by Eq. (34). Due to this relation, we can infer other parameters in the model Eqs. (3) and (4). From the relation between the dimensionless wave number κ and the dimensional wave number k,

$$\kappa^2=\frac{\alpha_1 D-\alpha_2}{2D}=\frac{D_1}{\sqrt{b_1 b_2}}k^2, \tag{39}$$

we get

$$\frac{2\pi}{\kappa_c}=12.6=\frac{2\pi}{k_c}\frac{\sqrt[4]{b_1 b_2}}{\sqrt{D_1}}. \tag{40}$$

The observed diameters of the brine channels range from μm to mm scale [9]. For a size of $2\pi/k_c=10$ μm and a diffusion coefficient $D_1=10^{-5}$ cm^2 s^{-1} for H_2O molecules, we obtain the product $b_1 b_2=2.5\times10^6$ s^{-2} and a transition rate $a_1=\sqrt{b_1 b_2}\alpha_1=1111$ s^{-1}. The rate a_1 is proportional to reorientations of the molecules per second, $1/\tau_d=10^5$ s^{-1} (Eisenberg) [26] and to the scaled temperature $\frac{T_c-T}{T_c}$,

$$a_1\sim\frac{T_c-T}{T_c}\frac{1}{\tau_d}, \tag{41}$$

where T_c is the melting point depending on the salinity. The mean salinity in sea ice of 35 g/l corresponds to 1 NaCl molecule per 100 H_2O molecules, i.e., 1 Na^+ ion and 1 Cl^- ion per 100 H_2O molecules in a diluted solution after the dissociation or a ratio of $x=(n_{Na^+}+n_{Cl^-})/n_{H_2O}=1/50$. From these facts, we obtain according to Clausius-Clapeyron

$$\Delta T=-\frac{xRT^2}{\Delta H}, \tag{42}$$

a freezing point depression from 0 to −2 °C, where $\Delta H=6$ kJ/mol is the latent heat of the phase transition from water to ice, $R=8.314$ J/mol K is the universal gas constant and $T=273$ K. Thus we obtain correctly $T_c=271$ K. For an environmental temperature of $T=-5$ °C$=268$ K according

to Eq. (41), a transition rate of $\frac{271-268}{271}\times 10^5\ \mathrm{s}^{-1}=1107\ \mathrm{s}^{-1}$ follows which nearly corresponds to $a_1=1111\ \mathrm{s}^{-1}$, which we estimated from the domain size (39).

Furthermore, we find the transition rate $a_2=\sqrt{b_1b_2}\alpha_2=1587\ \mathrm{s}^{-1}$ and the diffusion coefficient $D_2=6\times 10^{-5}\ \mathrm{cm}^2/\mathrm{s}$. Due to the transformation of Eq. (3) into the dimensionless form (5), there exists a fixed relation (11) because of $c=1$. We obtain for the Eq. (3) the rate d_c with $\alpha_1=a_1/\sqrt{b_1b_2}$, $\delta=d\sqrt{b_1b_2}/c^2$ of

$$d_c=\frac{3c^2}{16a_1}, \tag{43}$$

which is proportional to c^2. A transition rate $c=1000\ \mathrm{s}^{-1}$ yields a critical rate $d_c=169\ \mathrm{s}^{-1}$. From the knowledge of the diffusion coefficient D_1 and the size of brine channels, we can deduce the two rates a_1 and a_2. Both rates possess the same order of magnitude and are inside the Turing space of structure formation. If the experiments would lead to other parameters a_1 and a_2, especially to rather different values, a brine channel could not arise because of the limitation of the Turing space in Figs. 6 and 7. In other words, the model here seems to describe the experimental finding of brine channel formation.

Due to the small difference between the time constants a_1 and a_2, we obtain a dynamic interference between the reorientation of the water molecules and the desalinization. Both are evolving on nearly the same time scale. In particular, we cannot simplify the kinetics by separating time scales using the Tichonov theorem [34] known as steady-state hypothesis in order to reduce our reaction-diffusion systems (3) and (4) but have to consider both dynamics as demonstrated.

V. CONCLUSION

In this paper, it has been shown that a reaction-diffusion system which connects the basic ideas both of Ginzburg and of Turing can describe the formation of brine channels with realistic parameters. For the chosen parameters, patterns of similar size emerged. Eicken [35] and Weissenberger [9] distinguished between six various texture classes of sea ice dependent on the crystal morphology, brine inclusions, and the genesis. The different ice crystal growth depends on snow deposition, flooding, turbulent mixing, quiescent growth rate, or supercooling. Each condition determines the character of the kinetics. Nonlinear heat and salt dissipation, for example, lead to dendritic growth (snowflakes) whereas one observes in sea ice mostly lamellar or cellular structures rather than complete dendrits [7]. Hence, the morphology of sea ice is one criterion for the choice of an appropriate kinetics for the genesis of sea ice. Therefore, in order to simulate different structure sizes and textures, we can modify the dispersion relation by varying the parameters α_1, α_2, and D or by a modified kinetics [36]. The crucial point is the shape of the dispersion function. If there are multiple different positive unstable regions for the wave numbers with positive real part of eigenvalues, we could expect that differently large channels evolve. For instance Worster and Wettlaufer [20] presented a general theory for convection with mushy layers. The two different minima of the neutral curve, determined by the linear stability analysis, correspond to two different modes of convection, which affect the kinetics and determine the size distribution of the brine channels. We note that the initial conditions are decisive for the appearance of specific pattern [33]. Hence, one should investigate how dislocations or antifreeze proteins influence the formation of the brine channel distribution.

ACKNOWLEDGMENTS

The authors are deeply indebted Jürgen Weissenberger for the many exposures of casts brine channels. Dr. L. Dünkel and Dr. P. Augustin are thanked for their system theoretic discussion and Dr. U. Menzel at the Rudbeck laboratory, Uppsala, Sweden for his support. This work was supported by DFG Priority Program 1155, Grant No. GE1202/06by the DFG-CNPq Grant No. 444BRA-113/57/0-1, the BMBF, the DAAD, and by European ESF program NES. The financial support by the Brazilian Ministry of Science and Technology is acknowledged.

APPENDIX A: DIMENSIONLESS QUANTITIES

If we set $\tau=\frac{t}{t_0}$, $\xi=\frac{x}{x_0}$, $u=C_1\psi$, and $v=C_2\rho$, we get with $\frac{\partial\psi}{\partial t}=\frac{\partial\tau}{\partial t}\frac{\partial\psi}{\partial\tau}=\frac{1}{t_0}\frac{\partial\psi}{\partial\tau}$ and $\frac{\partial\psi}{\partial x}=\frac{\partial\xi}{\partial x}\frac{\partial\psi}{\partial\xi}=\frac{1}{x_0}\frac{\partial\psi}{\partial\xi}$,

$$\frac{\partial u}{\partial t}=C_1\frac{\partial\psi}{\partial t}=\frac{C_1}{t_0}\frac{\partial\psi}{\partial\tau} \tag{A1}$$

and

$$\frac{\partial u}{\partial x}=C_1\frac{\partial\psi}{\partial x}=\frac{C_1}{x_0}\frac{\partial\psi}{\partial\xi}. \tag{A2}$$

Because of $\frac{\partial^2\psi}{\partial\xi^2}=\frac{\partial^2\psi}{\partial x^2}\left(\frac{\partial x}{\partial\xi}\right)^2+\frac{\partial\psi}{\partial x}\frac{\partial^2 x}{\partial\xi^2}=x_0^2\frac{\partial^2\psi}{\partial x^2}$, we obtain $\frac{\partial^2\psi}{\partial x^2}=\frac{1}{x_0^2}\frac{\partial^2\psi}{\partial\xi^2}$ and consequently

$$\frac{\partial^2 u}{\partial x^2}=C_1\frac{\partial^2\psi}{\partial x^2}=\frac{C_1}{x_0^2}\frac{\partial^2\psi}{\partial\xi^2}. \tag{A3}$$

Accordingly one has

$$\frac{\partial v}{\partial t}=\frac{C_2}{t_0}\frac{\partial\rho}{\partial\tau},$$

$$\frac{\partial^2 v}{\partial x^2}=\frac{C_2}{x_0^2}\frac{\partial^2\rho}{\partial\xi^2}. \tag{A4}$$

From Eqs. (3) and (4) follow the dimensionless equations

$$\frac{\partial\psi}{\partial\tau}=f[\psi,\rho]+D_1\frac{t_0}{x_0^2}\frac{\partial^2\psi}{\partial\xi^2}, \tag{A5}$$

$$\frac{\partial\rho}{\partial\tau}=g[\psi,\rho]+D_2\frac{t_0}{x_0^2}\frac{\partial^2\rho}{\partial\xi^2}, \tag{A6}$$

with

$$f[\psi,\rho]=a_1t_0\psi-ct_0C_1^2\psi^3+dt_0C_1^4\psi^5+b_1t_0\frac{C_2}{C_1}\rho,$$

$$g[\psi,\rho] = -a_2 t_0 \rho - b_2 t_0 \frac{C_1}{C_2}\psi. \tag{A7}$$

If we choose

$$ct_0 C_1^2 = 1, \quad b_1 t_0 \frac{C_2}{C_1} = 1,$$

$$D_1 \frac{t_0}{x_0^2} = 1, \quad b_2 t_0 \frac{C_1}{C_2} = 1, \tag{A8}$$

we obtain $C_1 = \sqrt[4]{\frac{b_1 b_2}{c^2}}$, $C_2 = \sqrt[4]{\frac{b_2^3}{b_1 c^2}}$, $t_0 = \frac{1}{\sqrt{b_1 b_2}}$, and $x_0 = \sqrt[4]{\frac{D_1^2}{b_1 b_2}}$.

APPENDIX B: LINEAR STABILITY ANALYSIS

Let $\bar{\psi}$ and $\bar{\rho}$ denote small displacements from the equilibrium values ψ_0 and ρ_0 and write $\psi = \psi_0 + \bar{\psi}$ and $\rho = \rho_0 + \bar{\rho}$. With respect to Eqs. (5) and (6), we obtain

$$\bar{\psi}_\tau(\xi,\tau) = \alpha_1(\psi_0 + \bar{\psi}) - (\psi_0 + \bar{\psi})^3 + \delta(\psi_0 + \bar{\psi})^5 + \rho_0 + \bar{\rho} + \bar{\psi}_{\xi\xi}(\xi,\tau),$$

$$\bar{\rho}_\tau(\xi,\tau) = D\bar{\rho}_{\xi\xi}(\xi,\tau) - \alpha_2(\rho_0 + \bar{\rho}) - (\psi_0 + \bar{\psi}). \tag{B1}$$

If we consider only linear terms

$$\bar{\psi}_\tau(\xi,\tau) = \cdots + \alpha_1\bar{\psi} - 3\psi_0^2\bar{\psi} + 5\delta\psi_0^4\bar{\psi} + \bar{\rho} + \cdots + \bar{\psi}_{\xi\xi}(\xi,\tau),$$

$$\bar{\rho}_\tau(\xi,\tau) = \cdots - \bar{\psi} - \alpha_2\bar{\rho} + \cdots + D\bar{\rho}_{\xi\xi}(\xi,\tau), \tag{B2}$$

we get

$$\begin{pmatrix} \frac{\partial}{\partial\tau}\bar{\psi} \\ \frac{\partial}{\partial\tau}\bar{\rho} \end{pmatrix} = \underbrace{\begin{pmatrix} \alpha_1 - 3\psi_0^2 + 5\delta\psi_0^4 & 1 \\ -1 & -\alpha_2 \end{pmatrix}}_{J_{(\psi=\psi_0,\rho=\rho_0)}} \begin{pmatrix} \bar{\psi} \\ \bar{\rho} \end{pmatrix} + \begin{pmatrix} \frac{\partial^2}{\partial\xi^2} & 0 \\ 0 & D\frac{\partial^2}{\partial\xi^2} \end{pmatrix} \times \begin{pmatrix} \bar{\psi} \\ \bar{\rho} \end{pmatrix}, \tag{B3}$$

where $J_{(\psi=\psi_0,\rho=\rho_0)}$ is the Jacobian

$$J_{(\psi=\psi_0,\rho=\rho_0)} = \begin{pmatrix} f_\psi & f_\rho \\ g_\psi & g_\rho \end{pmatrix}_{(\psi=\psi_0,\rho=\rho_0)} = \begin{pmatrix} \alpha_1 - 3\psi_0^2 + 5\delta\psi_0^4 & 1 \\ -1 & -\alpha_2 \end{pmatrix}, \tag{B4}$$

which we can calculate also considering Eqs. (7) and (8).

Using the Fourier ansatz $\bar{\psi} = \psi_0\, exp(\lambda\tau + i\kappa\xi)$ and $\bar{\rho} = \rho_0\, exp(\lambda\tau + i\kappa\xi)$ in Eq. (15), we find

$$\begin{pmatrix} \lambda\bar{\psi}_i \\ \lambda\bar{\rho}_i \end{pmatrix} = \begin{pmatrix} \alpha_1 - 3\psi_0^2 + 5\delta\psi_0^4 & 1 \\ -1 & -\alpha_2 \end{pmatrix} \begin{pmatrix} \bar{\psi}_i \\ \bar{\rho}_i \end{pmatrix} + \begin{pmatrix} -\kappa^2 & 0 \\ 0 & -D\kappa^2 \end{pmatrix} \times \begin{pmatrix} \bar{\psi}_i \\ \bar{\rho}_i \end{pmatrix}. \tag{B5}$$

With $\psi_0 = 0$ and $\rho_0 = 0$, the eigenvalue equation

$$0 = \left[\begin{pmatrix} \kappa^2 - \alpha_1 & -1 \\ 1 & \alpha_2 + D\kappa^2 \end{pmatrix} + \begin{pmatrix} \lambda & 0 \\ 0 & \lambda \end{pmatrix} \right] \begin{pmatrix} \bar{\psi}_i \\ \bar{\rho}_i \end{pmatrix} \tag{B6}$$

follows with the characteristic equation

$$\begin{aligned} 0 &= \begin{vmatrix} \alpha_1 - \kappa^2 - \lambda & 1 \\ -1 & -\alpha_2 - D\kappa^2 - \lambda \end{vmatrix} \\ &= \lambda^2 + [\kappa^2(1+D) + \alpha_2 - \alpha_1]\lambda \\ &\quad + \underbrace{D\kappa^4 + (\alpha_2 - \alpha_1 D)\kappa^2 - \alpha_1\alpha_2 + 1}_{h(\kappa^2)}. \end{aligned} \tag{B7}$$

[1] R. Clausius, *Über den zweiten Hauptsatz der mechanischen Wärmetheorie* (Friedrich Vieweg und Sohn, Braunschweig, 1867).
[2] A. M. Turing, Philos. Trans. R. Soc. London, Ser. B **237**, 37 (1952).
[3] B. Light, G. A. Maykut, and T. C. Grenfell, J. Geophys. Res. **108**, 3051 (2003).
[4] C. Krembs, R. Gradinger, and M. Spindler, J. Exp. Mar. Biol. Ecol. **243**, 55 (2000).
[5] K. M. Golden, S. F. Ackley, and V. I. Lytle, Science **282**, 2238 (1998).
[6] D. K. Perovich and A. J. Gow, J. Geophys. Res. **96**, 16943 (1991).
[7] H. Eicken, in *Sea Ice: An Introduction to its Physics, Chemistry, Biology and Geology*, edited by D. N. Thomas and G. S. Dieckmann (Blackwell Science Ltd., Oxford, 2003), Chap. 2.
[8] H. Nada, J. P. van der Eerden, and Y. Furukawa, J. Cryst. Growth **266**, 297 (2004).
[9] J. Weissenberger, Berichte zur Polarforschung **111**, 1 (1992).
[10] A. Bartsch, Berichte zur Polarforschung **63**, 1 (1989).
[11] H. Trinks, W. Schröder, and C. K. Biebricher, Origins Life Evol. Biosphere **35**, 429 (2005).
[12] J. Weissenberger, G. Dieckmann, R. Gradinger, and M. Spindler, Limnol. Oceanogr. **37**, 179 (1992).
[13] D. K. Perovich and A. J. Gow, J. Geophys. Res. **101**, 18327 (1996).
[14] G. F. N. Cox, J. Glaciol. **29**, 425 (1983).
[15] G. F. N. Cox and W. F. Weeks, J. Glaciol. **29**, 306 (1983).
[16] G. F. N. Cox and W. F. Weeks, J. Geophys. Res. **93**, 12449 (1988).
[17] F. Cottier, H. Eicken, and P. Wadhams, J. Geophys. Res. **104**, 15859 (1999).
[18] C. J. Mundy, D. G. Barber, C. Michel, and R. F. Marsden, Polar Biol. **30**, 1099 (2007).
[19] C. Krembs, T. Mock, and R. Gradinger, Polar Biol. **24**, 356 (2001).
[20] M. G. Worster and J. S. Wettlaufer, J. Phys. Chem. B **101**, 6132 (1997).
[21] M. Fabrizio, J. Math. Phys. **49**, 102902 (2008).
[22] W. C. Röntgen, Ann. Phys. **45**, 91 (1892).
[23] D. M. Dennison, Phys. Rev. **17**, 20 (1921).
[24] W. H. Bragg, Proc. R. Soc. London **34**, 98 (1922).
[25] N. Bjerrum, Det Kongelige Danske Videnskabernes Selskab, Matematisk-fysiske Meddelelser **27**, 1 (1951).
[26] D. Eisenberg and W. Kauzmann, *The Structure and Properties of Water* (Clarendon Press, Oxford, 2005).
[27] N. N. Medvedev and Y. I. Naberukhin, J. Non-Cryst. Solids **94**, 402 (1987).
[28] H. E. Stanley, J. Phys. A **12**, L329 (1979).
[29] H. E. Stanley and J. Teixeira, J. Chem. Phys. **73**, 3404 (1980).
[30] Y. Kawano and T. Ohashi, Cold Regions Sci. Technol. **57**, 39 (2009).
[31] H. Haug, *Statistische Physik* (Friedr. Vieweg & Sohn Verlagsgesellschaft mbH, Braunschweig, 1997).
[32] R. Feistel and E. Hagen, Cold Regions Sci. Technol. **28**, 83 (1998).
[33] J. D. Murray, *Mathematical Biology* (Springer Verlag, Berlin, 1993).
[34] A. Tichonov, Mat. Sb. **31**, 575 (1952).
[35] H. Eicken, Berichte zur Polarforschung **82**, 1 (1991).
[36] G. Turk, Comput. Graph. **25**, 289 (1991).